Thermodynamic phase structure and topological charge of Hayward–AdS black holes under phase space constraints*

Qi-Hang Xia (夏启航)[1,2] Hui-Hua Zhao (赵惠华)[1,2] Meng-Sen Ma (马孟森)[1,2†]

[1]Department of Physics, Shanxi Datong University, Datong 037009, China
[2]Institute of Theoretical Physics, Shanxi Datong University, Datong 037009, China

Abstract: We investigate the thermodynamic behavior of the Hayward-AdS black hole and compare it with its singular counterpart, from which it is constructed by imposing an additional constraint. The singular black hole displays a rich phase structure, including reentrant phase transitions reminiscent of those observed in higher-dimensional Kerr-AdS spacetimes. After the constraint is imposed, the resulting Hayward-AdS black hole continues to exhibit Van der Waals–type $P-V$ criticality. However, its Gibbs free energy profile differs qualitatively from that of standard RN-AdS black holes. Additionally, we extend the analysis by employing thermodynamic topology to characterize the global structure of the phase space. We find that the topological charge of the singular black hole is -1, whereas that of the Hayward-AdS black hole is $+1$. This change in topological charge indicates that the constraint not only regularizes the geometry but also induces a qualitative transformation in the thermodynamic configuration space.

Keywords: black hole thermodynamics, regular black hole, topological charge

DOI: **CSTR:**

I. INTRODUCTION

Singularities are regarded as topological defects of spacetime in general relativity. Near spacetime singularities, the classical description of general relativity is expected to break down, and quantum gravitational effects become significant. The singularity is enclosed within the event horizon, preventing it from being exposed —this conclusion is known as the Weak Gravity Conjecture[1, 2].

Most black hole solutions derived from general relativity contain singularities. However, in 1968, Bardeen[3] obtained a non-singular solution within the framework of general relativity, which is referred to as a regular black hole. Subsequently, numerous scholars have constructed various types of regular black holes. For instance, Ayon Beato[4−6] and García developed charged regular black holes, taking nonlinear electrodynamics as the source of the field equations. Hayward[7] constructed a class of neutral regular black holes. Later, some researchers attributed the origin of regular black holes to the coupling between general relativity and nonlinear electrodynamics[8−22].

Additionally, extensive studies have been conducted on the thermodynamic properties of regular black holes[23−29]. However, when starting from the metric function of regular black holes, the first law of thermodynamics derived from the obtained mass, temperature, and entropy does not hold. To address this, we first construct a singular black hole. Then, by introducing a constraint condition, we obtain the solution for the singular black hole and further derive the solution for the Hayward-AdS black hole. Although the phase space of the thermodynamic quantities is reduced by one dimension, the constraint condition can be employed to establish a connection between the parameters of the Hayward-AdS black hole and those of the singular black hole. Ultimately, this method ensures that the thermodynamic parameters of the two black holes are highly consistent. The phase transition structures of the singular and regular black holes are investigated through temperature, heat capacity, and Gibbs free energy. The phase transition characteristics of these black holes are analogous to the liquid-gas phase transition described by the Van der Waals equation, as observed in the phase transition processes of RN-AdS and Gauss-Bonnet-AdS black holes. Furthermore, ther-

Received 27 February 2026; Accepted 1 June 2026

* This work is supported in part by Shanxi Provincial Natural Science Foundation of China (Grant No. 202203021221211) and the Scientific and Technological Innovation Programs of Higher Education Institutions in Shanxi (Grant No. 2021L386)

† E-mail: mengsenma@gmail.com

modynamic stability can be explored by means of thermodynamic topology methods[30–32].

This paper is organized as follows. In Section 2, we derive the solution for a singular black hole by employing nonlinear electrodynamics as the source for the field equations; this section is also devoted to calculating the corresponding thermodynamic quantities of the singular black hole and analyzing its phase structure. In Section 3, we incorporate the constraint obtained from the singular black hole into the Hayward-AdS black hole framework. We then calculate the relevant thermodynamic quantities for the Hayward-AdS black hole and examine its phase structure. In Section 4, we analyze the thermodynamic topology of the singular and regular black holes. Finally, we summarize the research findings and discuss potential avenues for future work in Section 5.

II. THE SINGULAR BLACK HOLE AND ITS THERMODYNAMIC PROPERTIES

We begin by constructing a singular black hole solution in Einstein gravity coupled to a nonlinear electrodynamics source in the presence of a cosmological constant. The relevant Einstein field equations are

$$G_{\mu\nu}+\Lambda g_{\mu\nu}=8\pi T_{\mu\nu}. \tag{1}$$

We adopt the static, spherically symmetric metric ansatz

$$ds^2=-f(r)dt^2+f(r)^{-1}dr^2+r^2d\Omega^2. \tag{2}$$

Without loss of generality, we consider the metric function to be of the form:

$$f(r)=1-\frac{2m(r)}{r}. \tag{3}$$

Inserting this ansatz into the field equations yields

$$-\frac{2m'(r)}{r^2}+\Lambda=8\pi T^0_0. \tag{4}$$

The integrated form of the equation is

$$m(r)=M+4\pi\int_r^\infty r^2T^0_0dr+\frac{\Lambda}{6}r^3, \tag{5}$$

where M is an integration constant, which is just the ADM mass in asymptotically flat spacetime.

We consider a nonlinear electrodynamic matter field as the gravitational source, whose Lagrangian takes the form[33]

$$\mathcal{L}=\frac{4\mu}{\alpha}\frac{(\alpha F)^{\frac{\mu+3}{4}}}{\left[1+(\alpha F)^{\frac{\mu}{2}}\right]^2}, \tag{6}$$

where F is defined as $F=F_{\mu\nu}F^{\mu\nu}$, $\mu=3$, and α is a positive coupling constant with dimensions of $[L]^2$.

In the spherically symmetric case with a pure magnetic field, $F_{\mu\nu}$ involves a radial magnetic field F_{23} and satisfies

$$F_{23}=Q\sin\theta, \tag{7}$$

where Q is the magnetic charge. Thus, $F=2F_{23}F^{23}=\frac{2Q^2}{r^4}$.

The energy-momentum tensor derived from $\mathcal{L}(F)$ is

$$T_{\alpha\beta}=g_{\alpha\beta}\mathcal{L}+4\mathcal{L}_F F_{\alpha\mu}F^{\mu}_{\beta}, \tag{8}$$

where $\mathcal{L}_F\equiv\partial\mathcal{L}/\partial F$. In the static, spherically symmetric case, we have $T^0_0=\mathcal{L}$.

Now, from Eq. (5) we obtain

$$m(r)=M-\frac{32\sqrt{2}\pi Q^3\sqrt{\alpha}}{r^3+2^{3/4}(Q^2\alpha)^{3/4}}+\frac{\Lambda}{6}r^3, \tag{9}$$

Therefore, the metric function takes the form

$$f(r)=1-\frac{2M}{r}-\frac{\Lambda r^2}{3}+\frac{64\sqrt{2\alpha}\pi Q^3}{r^4+(2Q^2\alpha)^{3/4}r}. \tag{10}$$

We now investigate the thermodynamic properties of this singular black hole. The Hawking temperature can be directly derived from the metric function,

$$T=\frac{r_+^6\left(1-\Lambda r_+^2\right)+2\sqrt{2}Q^3\sqrt{\alpha}\left[\alpha-(96\pi+\alpha\Lambda)r_+^2+(2\alpha)^{1/4}(r_+^3-\Lambda r_+^5)\right]}{4\pi r_+\left[2^{3/4}(Q^2\alpha)^{3/4}+r_+^3\right]^2}, \tag{11}$$

Regardless of the values of (Q,Λ,α), the temperature always diverges in the limit $r_+\to 0$.

In the present work, we focus on the extended phase space, where both dimensional parameters are integrated into the thermodynamic phase space of the black hole[34]. Specifically, the cosmological constant is

treated as the thermodynamic pressure $P=-\Lambda/8\pi$[35]. It can be verified that the first law of black hole thermodynamics holds in this case.

$$dM = TdS + \Phi dQ + \mathcal{A}d\alpha + VdP, \tag{12}$$

where $S=A/4$, and $\Phi,\mathcal{A},V$ are the conjugate quantities of Q,α,P, respectively.

From Eq. (11), we can obtain the pressure as a function of (T,r_+,α,Q):

$$P=\frac{-2\sqrt{2}Q^3\alpha^{3/2}+8\sqrt{2}A^{3/2}\pi Tr_+ +192\sqrt{2}\pi Q^3\sqrt{\alpha}r_+^2-2^{7/4}A^{3/4}r_+^3+2^{15/4}A^{3/4}\pi Tr_+^4-r_+^6+4\pi Tr_+^7}{8\pi r_+^2\left(2\sqrt{2}Q^3\alpha^{3/2}+2^{7/4}A^{3/4}r_+^3+r_+^6\right)}, \tag{13}$$

$$A=Q^3\alpha, \tag{14}$$

For comparison with the Van der Waals equation, for instance, when the specific volume satisfies $v=2r_+$, we can consider the $P-r_+$ criticality.

We can now study the P-V criticality of the black hole. Since P is a function of (T,r_+,Q), we set its first and second derivatives with respect to r_+ equal to zero. If critical points exist, we obtain the following conditions:

$$\frac{\partial P}{\partial r_+}=0, \quad \frac{\partial^2 P}{\partial r_+^2}=0. \tag{15}$$

Galois theory states that algebraic equations of degree five or higher generally lack radical solutions. The algebraic equations obtained here are too complex to be solved by radicals; therefore, we set $Q=0.01$ and $\alpha=2$ to derive a set of numerical solutions.

$$T_c=0.365, \quad r_{+c}=0.336, \quad P_c=0.022. \tag{16}$$

Its $P-r_+$ criticality is shown in Fig. 1. Compared with the RN-AdS black hole, this black hole exhibits an additional branch in the small black hole region. Its behavior is similar to that of the higher-dimensional rotating-AdS black holes [36] and the Gauss-Bonnet-AdS black hole [37]. In Fig. 1, we also depict the $T-r_+$ curves. Only when $P>0$ does the temperature tend to infinity as $r_+\to\infty$. When $P<P_c$, the temperature also exhibits four branches, corresponding to the $P-r_+$ curve when $T<T_c$.

Next, we examine the heat capacity, which not only characterizes the local thermodynamic stability but also provides insights into the microscopic degrees of freedom of the black hole. We calculate the heat capacity at constant (Q,P,α):

$$C=\left.\frac{\partial M}{\partial T}\right|_{Q,P,\alpha}. \tag{17}$$

Regarding the stability of a black hole, a positive heat capacity indicates thermodynamic stability, whereas a negative heat capacity indicates thermodynamic instability. For fixed Q, α, and P, three divergent points appear in the heat capacity when $P_0>P$. These divergent points correspond to the extrema of the temperature. Specifically, the heat capacities of the small and large black holes are positive (thermodynamically stable), whereas those of the intermediate and smallest black holes are negative (thermodynamically unstable).

When $P>P_c$, the two divergent points on the right side vanish (Fig. 2c and Fig. 2d). There exists a particu-

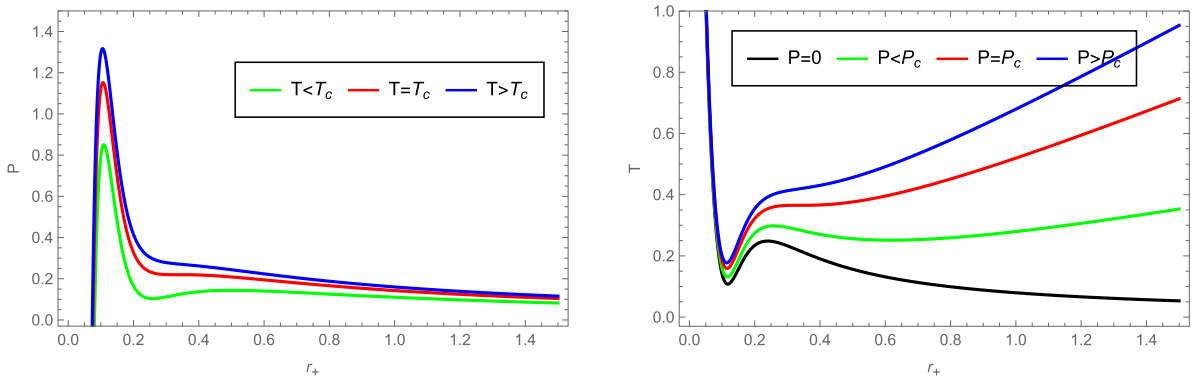

Fig. 1. (color online) The $P-r_+$ and $T-r_+$ curves of the singular black hole for fixed $Q=0.01$ and $\alpha=2$.

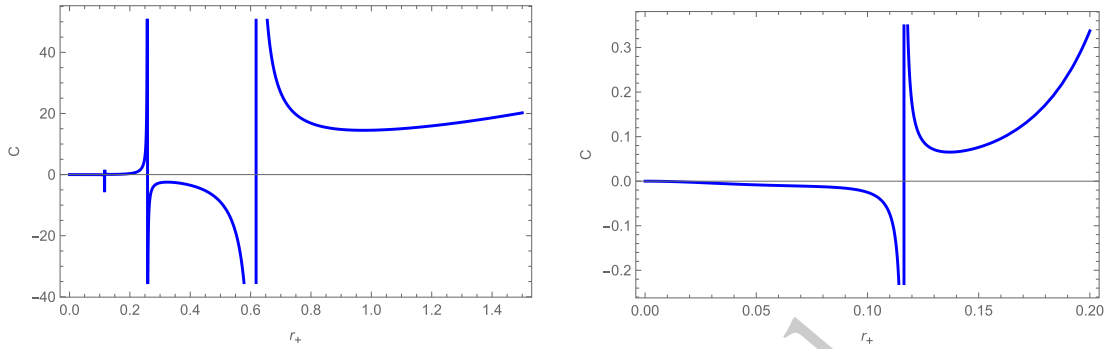

(a) $P = 0.1 < P_c$ (b) Magnification of (a) in the $[0, 0.2]$

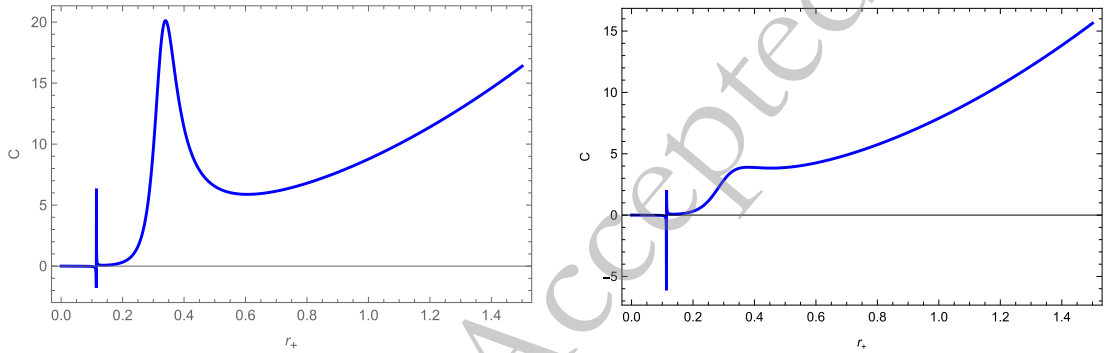

(c) $P = 0.24 < P_0$ (d) $P = 0.35 > P_0$

Fig. 2. (color online) The behavior of $C - r_+$ for the singular black hole for different values of P at fixed $Q = 0.01$ and $\alpha = 2$. Here, $P_0 = 0.32$.

lar pressure, denoted by P_0. When $P < P_0$, the heat capacity exhibits a pronounced peak, a behavior reminiscent of the Schottky anomaly. This feature may suggest the existence of discrete energy levels within the black hole's underlying microstructure [38]. For pressures $P \geq P_0$, the peak vanishes, as is shown in Fig. 2d. The heat capacity curve exhibits two plateaus, analogous to the heat capacity characteristics observed in a diatomic ideal gas.

According to the first law, in the fixed (Q, P, α) ensemble, we can define the Gibbs free energy as

$$G = M - TS. \tag{18}$$

As shown in Fig. 3, there exist two special pressures, namely P_0 and P_z. When $P < P_0$, the large black hole phase exists at low temperatures. When $P_0 < P < P_z$, a zeroth-order phase transition occurs. When $P_z < P < P_c$, a swallowtail structure emerges, indicating that the thermodynamic transition evolves from a zeroth-order phase transition to a first-order phase transition. As the temperature increases, the black hole transforms from the small black hole phase to the large black hole phase [39–45].

III. THERMODYNAMICS OF THE HAYWARD-ADS BLACK HOLE

Expanding the singular metric function, Eq. (10), near $r = 0$, one finds that

$$f(r) = 1 - \frac{1}{r}\left[2M - \frac{64\sqrt{2}\pi Q^3\sqrt{\alpha}}{2^{3/4}(Q^2\alpha)^{3/4}}\right] - \frac{\Lambda r^2}{3} + O\left(r^2\right). \tag{19}$$

To eliminate the physical singular point, one can impose a regular constraint condition, namely

$$M = \frac{16\times 2^{3/4}\pi Q^{3/2}}{\alpha^{1/4}}. \tag{20}$$

Combined with the metric function, it can be equivalently written as

$$Q = \frac{1}{\sqrt{2}}\left[\frac{3r_+^3 - r_+^5\Lambda}{\alpha^{1/2}(96\pi + \alpha\Lambda)r_+^2 - 3\alpha}\right]^{2/3}, \tag{21}$$

In this way, we obtain the Hayward-AdS black hole,

$$\begin{aligned} f(r) &= 1 - \frac{32\times 2^{3/4}\pi Q r^2\left(Q^2\alpha\right)^{1/4}}{\sqrt{\alpha}\left[r^3 + 2^{3/4}(Q^2\alpha)^{3/4}\right]} - \frac{r^2\Lambda}{3} \\ &= 1 - \frac{32M\pi r^2}{16\pi r^3 + M\alpha} - \frac{r^2\Lambda}{3}. \end{aligned} \tag{22}$$

The nature of this solution as a regular black hole can be

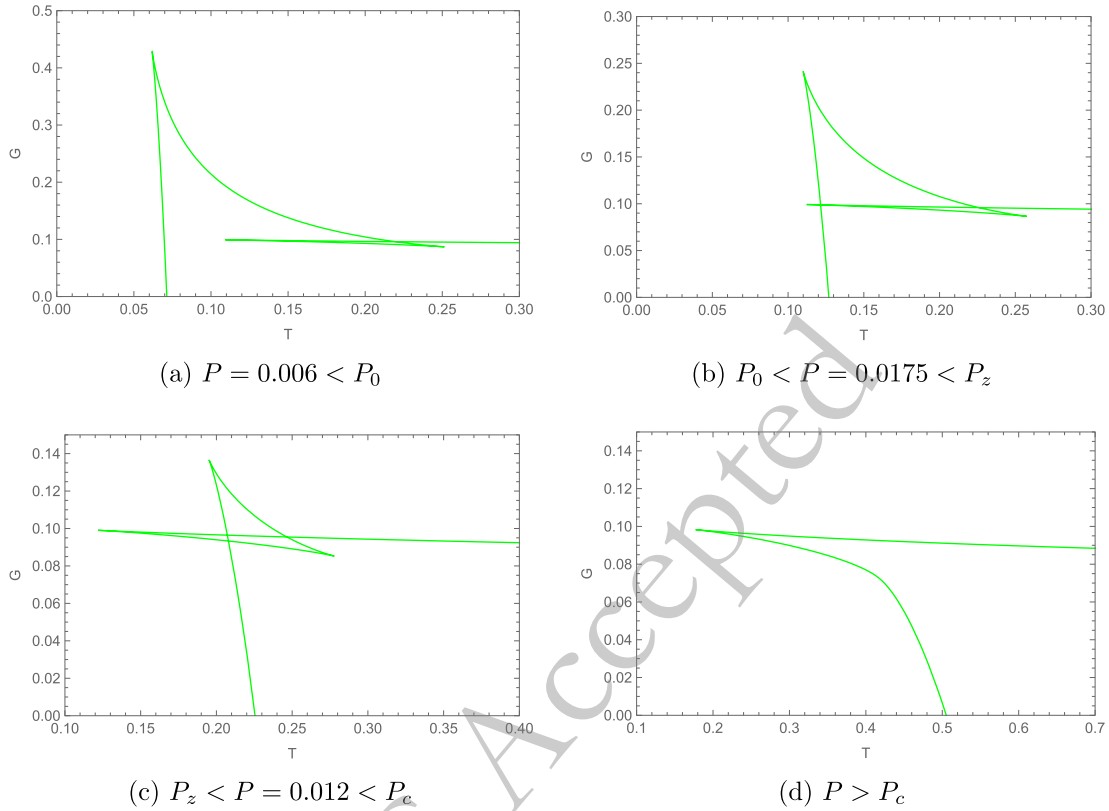

(a) $P = 0.006 < P_0$ (b) $P_0 < P = 0.0175 < P_z$

(c) $P_z < P = 0.012 < P_e$ (d) $P > P_c$

Fig. 3. (color online) The $G-T$ curves of the singular black hole for different values of P at fixed $Q = 0.01$ and $\alpha = 2$. Here, $P_z = 0.018$ and $P_0 = 0.016$.

verified by calculating the Kretschmann scalar. Specifically, setting $\Lambda = 0$ recovers the Hayward regular black hole.

The temperature of the present regular black hole can be derived from the metric function (22), or obtained directly by applying the constraint (21) to Eq.(11),

$$\text{Eq.(11)} \xrightarrow{(21)} T = -\frac{\alpha\left(-3+\Lambda r_+^2\right)^2 + 96\pi r_+^2\left(\Lambda r_+^2 - 1\right)}{384\pi^2 r_+^3}. \quad (23)$$

Therefore, we conjecture that the temperature of the Hayward-AdS black hole behaves differently from that of its singular counterpart. Using this temperature, we can derive the pressure P as a function of (T, r_+, α).

$$\text{Eq.(13)} \xrightarrow{(21)} P = \frac{-3}{\alpha r_+}\left(-2r_+ + \frac{\alpha}{8\pi r_+} + \frac{\sqrt{12\pi r_+^2 - \alpha - 2\pi r T\alpha}}{\sqrt{3\pi}}\right). \quad (24)$$

In Fig. 4, we depict the $T-r_+$ and $P-r_+$ curves. Superficially, it appears that the Hayward-AdS black hole exhibits critical behavior similar to that of the RN-AdS black hole[46]. We can also calculate the critical point for a fixed $\alpha = 2$:

$$T_c = 0.164, \quad r_{+c} = 0.614, \quad P_c = 0.051. \quad (25)$$

However, we note that the introduction of the additional constraint causes the thermodynamic variables to no longer be independent, thereby invalidating the first law of thermodynamics. In this case, the heat capacity defined in accordance with the first law of thermodynamics is no longer valid. To obtain the correct heat capacity of the Hayward-AdS black hole, we follow the same approach used for the temperature mentioned above.

$$\text{Eq.(17)} \xrightarrow{(21)} C, \quad (26)$$

This is because, in this case

$$C \neq \frac{\partial M}{\partial T} = \frac{\partial M/\partial r_+}{\partial T/\partial r_+}. \quad (27)$$

For $\alpha = 2$, we find three real solutions when $P = 0.03 < P_c$. This is depicted in Figs. 5a and 5b. The first divergent point occurs in the region where the temperature is negative, and thus should be excluded. When $P = P_c = 0.051$, the heat capacity is consistently positive within the region of positive temperature, and no divergent points exist (Fig. 5c and 5d).

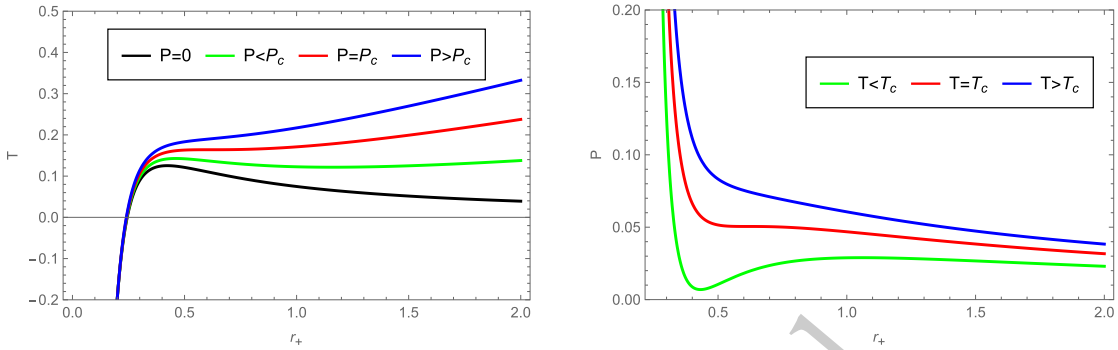

Fig. 4. (color online) The $T-r_+$ and $P-r_+$ curves of the Hayward-AdS black hole for fixed $\alpha=2$.

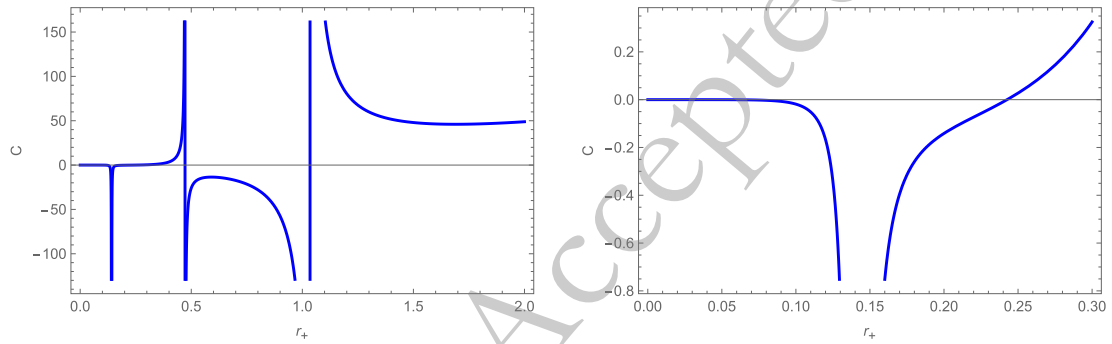

(a) $P=0.03<P_c$ (b) Magnification of (a) in the $[0,0.3]$

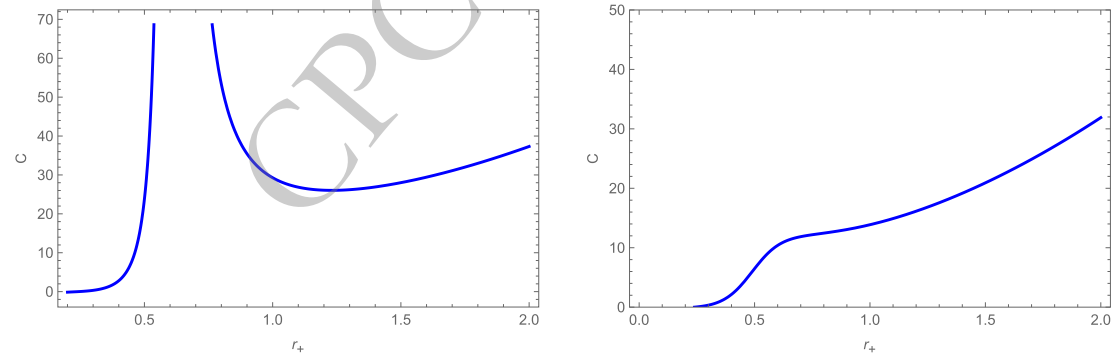

(c) $P=P_c=0.051$ (d) $P=0.09$

Fig. 5. (color online) The behavior of $C-r_+$ for the Hayward-AdS black holes with fixed $\alpha=2$.

The Gibbs function is defined based on the first law of thermodynamics and the Legendre transformation. Since the first law of thermodynamics is invalid, we cannot directly define the Gibbs function of the Hayward-AdS black hole in accordance with this law and the Legendre transformation. Since the standard first-law form is not preserved under naive reduction, the ordinary Gibbs potential defined by an unconstrained Legendre transformation on the reduced variables is not appropriate. Instead, we use the pullback of the Gibbs free energy defined in the full phase space and refer to it as the induced Gibbs potential. Following the same approach used to define the temperature above, we can ultimately obtain it by introducing an additional constraint

$$\text{Eq.(18)} \xrightarrow{(21)} G=-\frac{1}{4}r_+\left(1+8P\pi r_+^2\right)+\frac{\alpha\left(3+8P\pi r_+^2\right)^2}{384\pi r_+} -\frac{16\pi r_+^3\left(3+8P\pi r_+^2\right)}{3\alpha+8(P\alpha-12)\pi r_+^2}. \tag{28}$$

As illustrated in Fig. 6, when $P\geq P_c$, the Gibbs free energy exhibits only one branch, whereas when $P<P_c$, three branches emerge corresponding to the temperatures. It is evident that the characteristics of the $G-T$ curves differ from those of the RN-AdS black hole. No "swallow tail" structure exists for $P<P_c$; instead, an "8-shaped" knot is observed.

Indeed, the Hayward-AdS black hole exhibits a more

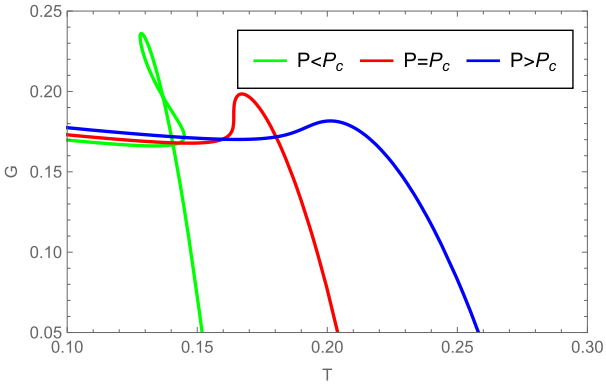

Fig. 6. (color online) The $G-T$ curves for a fixed $\alpha=2$, taking P_c as the benchmark.

diverse phase structure. When $P=0$, the large black hole branch vanishes, a previously discussed phenomenon. As illustrated in Fig. 7c, there exists another specific pressure value, $P=0.028$, below which the $G-T$ curves display an "8"-like shape. When $0<P<0.032$, the upper loop of the "8"-shape contracts while the lower loop expands, transforming the "8"-shape into a swallowtail-like profile (Fig. 7a). It is important to emphasize that thermodynamic instability only emerges in a local segment of the intermediate branch, rather than across the entire branch. This characteristic also differentiates the Hayward-AdS black hole from Reissner-Nordström-AdS (RN-AdS) black holes and other AdS black hole variants. At $P=0.032$, the lower loop of the "8"-like shape disappears, and the curve evolves into a "0"-like shape. When $P=0.04<P_c$, the loop splits and develops into a "C"-shaped structure. In this case, a zeroth-order phase transition occurs between the small and large black holes.

It should be noted that although the Hayward-AdS black hole is obtained by imposing a regularity constraint on the singular black hole, this does not imply that the singular black hole is an absolutely fundamental solution. Rather, it represents the minimal unconstrained solution family within the same Einstein-NED model, from which the regular Hayward-AdS geometry can be obtained by imposing the regularity condition.

IV. THERMODYNAMIC TOPOLOGY

The thermodynamics of the extended phase space demonstrates an exact correspondence between the large/small phase transition of AdS black holes and the gas/liquid phase transition. Based on Duan Yishi's ϕ-mapping topological current theory, a vector field is constructed, where the zero points are regarded as topological defects. Topological current charges are used to study the properties of the black hole thermodynamic phase space. By relating the ϕ-mapping topological current to the order parameter, a topological invariant is obtained by analyzing the direction and coincidence degree of the winding number of the vector field's singularities via the Hopf

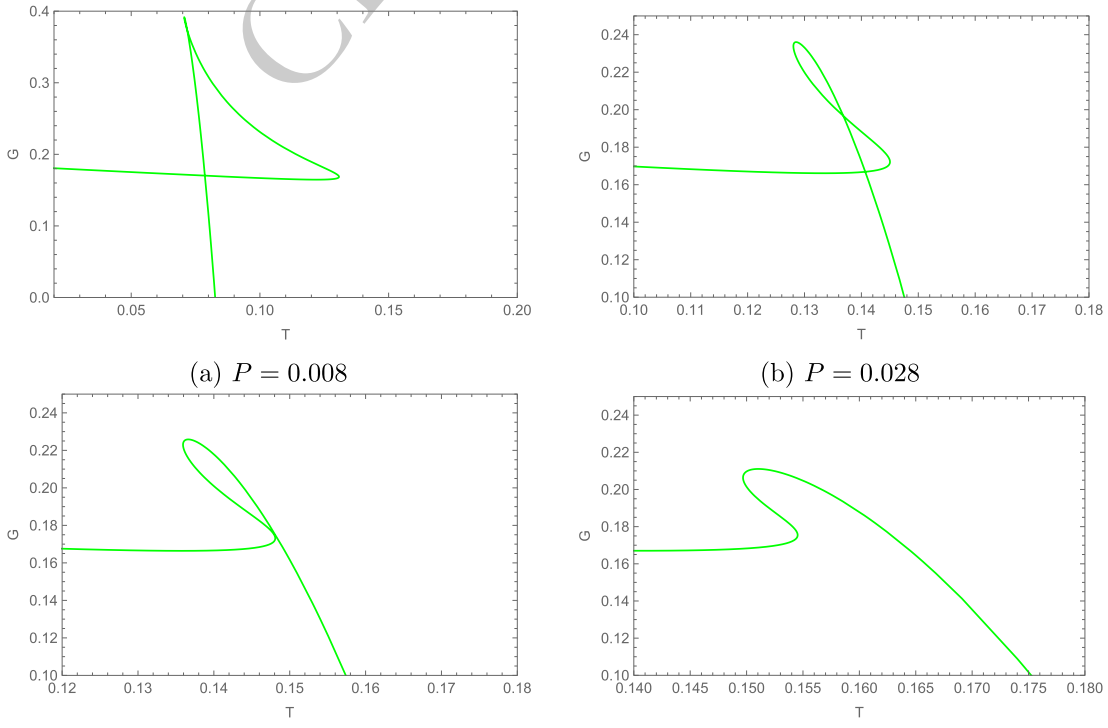

(a) $P=0.008$ (b) $P=0.028$

(c) $P=0.032$ (d) $P=0.04<P_c$

Fig. 7. (color online) The $G-T$ curves for fixed $\alpha=2$.

index and the Brouwer degree. This topological invariant can determine the stable, unstable, and metastable phases of black hole thermodynamics[47−50]. In this framework, the Helmholtz free energy is introduced, where $\tau = \frac{1}{T}$ (the inverse temperature) also serves as a period.

$$\mathcal{F} = M - \frac{S}{\tau}, \tag{29}$$

where M denotes the ADM mass; the vector field $\phi = \left(\phi^{r_+}, \phi^{\Theta}\right)$ is constructed by

$$\phi = \left(\frac{\partial \mathcal{F}}{\partial r_+}, -\cot\Theta \csc\Theta\right), \tag{30}$$

where Θ is an auxiliary angular coordinate introduced in the thermodynamic-topology construction for convenience. Its range is $0 \le \Theta \le \pi$. The divergence occurs at $\Theta = 0$ or $\Theta = \pi$, acting as two boundaries of the vector field, with the vector direction perpendicular to the horizontal lines and pointing outward. At $\phi^{r_h} = 0$ and $\Theta = \pi/2$, the Helmholtz free energy corresponds to the on-shell free energy, and the critical point is exactly located at the zero point of the vector field.

The topological current charge is given by j^μ

$$j^\mu = \frac{1}{2\pi}\epsilon^{\mu\nu\rho}\epsilon^{ab}\partial_\nu n^a \partial_\rho n^b, \quad n^a = \frac{\phi^a}{|\phi|}, \tag{31}$$

where $\mu,\nu,\rho = 0,1,2$ and $a,b \in \{1,2\}$. When $\partial_\mu j^\mu = 0$, corresponding to the zeros of the vector field ϕ, the total topological invariant (winding number) is obtained via a surface integral

$$W = \int_\Sigma j^0 d^2x = \sum_{i=1}^{n} \zeta_i \eta_i, \tag{32}$$

where ζ_i is the Hopf index and η_i is the sign of the Jacobian determinant evaluated at the i-th zero of ϕ.

Let us now calculate the thermodynamic topology of regular black holes and singular black holes. For the singular black holes, the generalized Helmholtz free energy is given by

$$\mathcal{F} = \frac{3r^4 + 8P\pi r^6 + 192\sqrt{2}\pi Q^3\sqrt{\alpha} + 3\times 2^{3/4} r\left(Q^2\alpha\right)^{3/4} + 8\times 2^{3/4} P\pi r^3 \left(Q^2\alpha\right)^{3/4}}{6r^3 + 6\times 2^{3/4}\left(Q^2\alpha\right)^{3/4}} - \frac{\pi r^2}{\tau}, \tag{33}$$

Additionally, using (30), we explicitly determine the components of the vector field ϕ as

$$\phi^{r_+} = \frac{\partial \mathcal{F}}{\partial r_+}, \tag{34}$$

We can readily calculate τ by equating them to zero.

$$\tau = \frac{-4\pi r_+^7 - 8\sqrt{2}\left(Q^2\alpha\right)^{3/4} r_+ \left(Q^{3/2}\alpha^{3/4} + 2^{1/4} r_+^3\right)}{2\sqrt{2}Q^3\sqrt{\alpha}\left(96\pi r_+^2 - \alpha - 8P\alpha r_+\right) - \left(1 + 8Pr_+^2\right)\left(2\times 2^{3/4}\left(Q^2\alpha\right)^{3/4} + r_+^6\right)}, \tag{35}$$

For the regular Hayward-AdS black hole, we obtain the following results:

$$\tau = \frac{1}{T} \neq \frac{\partial S}{\partial M}, \tag{36}$$

$$M = \frac{16\pi\left(3r^3 + 8P\pi r^5\right)}{96\pi r^2 - 3\alpha - 8P\pi r^2\alpha}, \tag{37}$$

$$\mathcal{F} = M - \frac{S}{\tau}, \tag{38}$$

$$\tau = \frac{2\left(-96\pi r^2 + 3\alpha + 8Pr^2\alpha\right)^2}{4608\pi r^3 + 36864P\pi^2 r^5 - 432\alpha - 2304Pr^3\alpha - 3072P^2\pi^2 r^5\alpha}, \tag{39}$$

We now investigate the thermodynamic topology of this type of black hole and employ vector diagrams to visualize the distribution of topological charges. We have plotted the plane. For the topological charges in Fig. 8a and 8b, the points surrounded by red contours represent the zero points in Fig. 8a. Their winding numbers are -1 and +1, corresponding to the thermodynamically unstable and stable branches, respectively, with a total winding number of zero. Similarly, for the topological charges in Fig. 8c and 8d, the points surrounded by red contours repres-

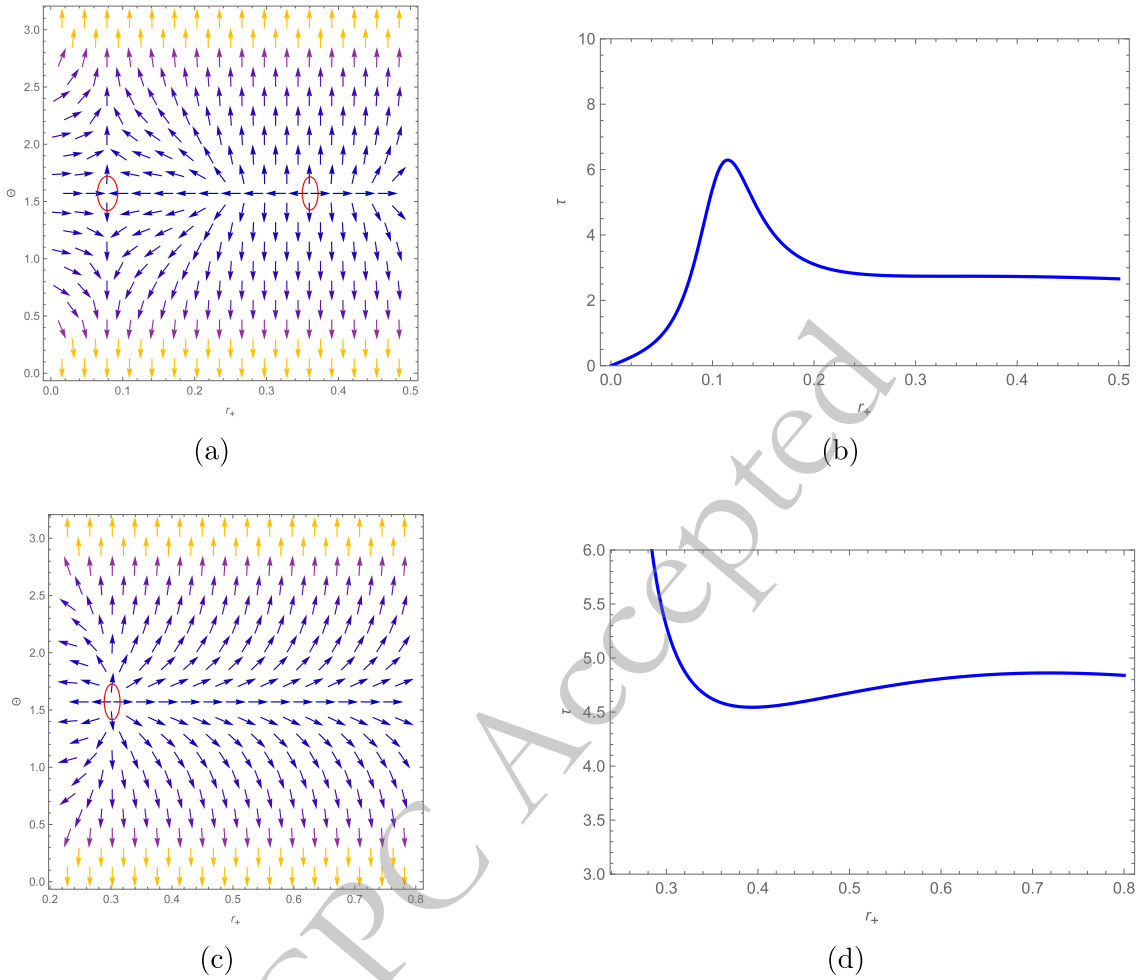

Fig. 8. (color online) Singular black hole in (a) and (b): $Q=0.01$, $\alpha=2$, $P_c=0.22$, and $\tau_c=2.74$; Regular black hole in (c) and (d): $\alpha=2$, $P_c=0.067$, and $\tau_c=5.28$.

ent the zero points in Fig. 8c. Their winding numbers are +1, corresponding to the thermodynamically stable branches.

V. DISCUSSIONS AND CONCLUSIONS

In this paper, we have investigated the properties of the regular Hayward-AdS black hole and its singular counterpart. The solution for the regular black hole is derived from the singular black hole by imposing a specific constraint. This constraint induces significant modifications to the thermodynamic behavior.

The singular black hole exhibits a rich phase structure, featuring both first-order and zeroth-order phase transitions. While the singular black hole displays $P-V$ criticality analogous to that of the RN-AdS black hole, the regular Hayward-AdS black hole, which is obtained from the singular black hole via the constraint, does not exhibit similar phase transition characteristics. Specifically, as the pressure varies below the critical pressure $P<P_c$, the $G-T$ diagram evolves sequentially through distinct topologies: first an "8-shaped" structure, followed by a "zero-like" single loop, and finally a "C-shaped" structure. The emergence of the "C-shaped" structure signifies a zeroth-order phase transition between the small and large black hole phases. However, for $P>P_c$, no phase transition features are observed.

Furthermore, we have analyzed the thermodynamic stability of both the singular black hole and the Hayward-AdS black hole. While the singular black holes share a total winding number of zero and the winding number of the Hayward-AdS black hole is +1, this does not necessarily imply identical thermodynamic stability. This issue warrants further consideration.

CONFLICT OF INTEREST

The authors declare that they have no known competing financial interests or personal relationships that could have appeared to influence the work reported in this paper.

DATA AVAILABILITY

No data was used for the research described in the article.

ACKNOWLEDGMENTS

We thank the anonymous reviewers for their careful reading of our manuscript and their many insightful comments and suggestions.

References

[1] N. Arkani-Hamed, Y.-t. Huang, J.-Y. Liu and G. N. Remmen, JHEP **03**, 083 (2022)
[2] D. Harlow, B. Heidenreich, M. Reece and T. Rudelius, Rev. Mod. Phys. **95**, 035003 (2023)
[3] J. Bardeen, *Non-singular general relativistic gravitational collapse, Proc. GR5 (Tbilisi, USSR)* (Sept., 1968) 174.
[4] E. Ayón-Beato and A. García, Phys. Rev. Lett. **80**, 5056 (1998)
[5] E. Ayón-Beato and A. García, Phys. Lett. B **464**, 25 (1999)
[6] E. Ayón-Beato and A. García, Phys. Lett. B **493**, 149 (2000)
[7] S. A. Hayward, Phys. Rev. Lett. **96**, 031103 (2006)
[8] K. A. Bronnikov, Phys. Rev. D **63**, 044005 (2001)
[9] A. Burinskii and S. R. Hildebrandt, Phys. Rev. D **65**, 104017 (2002)
[10] I. Dymnikova, Class. Quantum Grav. **21**, 4417 (2004)
[11] N. Bretón, Gen. Relativ. Gravit. **37**, 643 (2005)
[12] W. Berej, J. Matyjasek, D. Tryniecki and M. Woronowicz, Gen. Relativ. Gravit. **38**, 885 (2006)
[13] L. Balart and E. C. Vagenas, Phys. Rev. D **90**, 124045 (2014)
[14] M.-S. Ma, Annals of Physics **362**, 529 (2015)
[15] M. E. Rodrigues, E. L. B. Junior, G. T. Marques and V. T. Zanchin, Phys. Rev. D **94**, 024062 (2016)
[16] S. Nojiri and S. D. Odintsov, Phys. Rev. D **96**, 104008 (2017)
[17] Y. He and M.-S. Ma, Phys. Lett. B **774**, 229 (2017)
[18] S. G. Ghosh, D. V. Singh and S. D. Maharaj, Phys. Rev. D **97**, 104050 (2018)
[19] L. Gulin and I. Smolić, Classical and Quantum Gravity **35**, 025015 (2018)
[20] A. Bokulić, I. Smolić and T. Jurić, Physical Review D **103**, 124059 (2021)
[21] H. Maeda, J. High Energ. Phys. **2022**, 108 (2022)
[22] Z.-C. Li and H. Lü, Phys. Rev. D **110**, 104046 (2024)
[23] M.-S. Ma and R. Zhao, Class. Quantum Grav. **31**, 245014 (2014)
[24] R. Tharanath, J. Suresh and V. C. Kuriakose, Gen. Rel. Grav. **47**, 46 (2015)
[25] B. Pourhassan, M. Faizal and U. Debnath, Eur. Phys. J. C **76**, 145 (2016)
[26] C. Li, C. Fang, M. He, J. Ding and J. Deng, Mod. Phys. Lett. A **34**, 1950336 (2019)
[27] M. Molina and J. R. Villanueva, Class. Quant. Grav. **38**, 105002 (2021)
[28] M.-S. Ma, Y. He, X.-M. Wang and H.-F. Li, Phys. Lett. B **870**, 139961 (2025)
[29] M.-S. Ma, H.-F. Li and J.-H. Shi, Sci. China Phys. Mech. Astron. **69**, 210411 (2026)
[30] A. Anand, S. Noori Gashti and A. Singh, Phys. Dark Univ. **49**, 101994 (2025)
[31] W. Liu, L. Zhang, D. Wu and J. Wang, Class. Quant. Grav. **42**, 125007 (2025)
[32] S.-X. Bao, Z.-J. Wan and Y.-Z. Du, Commun. Theor. Phys. **78**, 015402 (2026)
[33] Z.-Y. Fan and X. Wang, Phys. Rev. D **94**, 124027 (2016)
[34] D. Kastor, S. Ray and J. Traschen, Classical and Quantum Gravity **26**, 195011 (2009)
[35] B. P. Dolan, Classical and Quantum Gravity **28**, 235017 (2011)
[36] N. Altamirano, D. Kubizňák and R. B. Mann, Physical Review D **88**, 101502 (2013)
[37] S.-W. Wei and Y.-X. Liu, Physical Review D **90**, 044057 (2014)
[38] J. Dinsmore, P. Draper, D. Kastor, Y. Qiu and J. Traschen, Chinese Physics C **37**, 054001 (2020)
[39] A. M. Frassino, D. Kubizňák, R. B. Mann and F. Simovic, Journal of High Energy Physics **2014**, 080 (2014)
[40] R. Hennigar and R. Mann, Entropy **17**, 8056 (2015)
[41] X.-X. Zeng and L.-F. Li, Phys. Lett. B **764**, 100 (2017), arXiv: 1512.08855
[42] X.-X. Zeng, H. Zhang and L.-F. Li, Phys. Lett. B **756**, 170 (2016), arXiv: 1511.00383
[43] M.-S. Ma and R.-H. Wang, Physical Review D **96**, 024052 (2017)
[44] D.-C. Zou, R. Yue and M. Zhang, The European Physical Journal C **77**, 256 (2017)
[45] M.-S. Ma and Y.-S. Liu, *Phase Transitions of GUP-Corrected Charged AdS Black Hole*, *Advances in High Energy Physics* **2018** (2018).
[46] D. Kubizňák and R. B. Mann, Journal of High Energy Physics **2012**, 033 (2012)
[47] S.-W. Wei, Y.-X. Liu and R. B. Mann, Phys. Rev. Lett. **129**, 191101 (2022)
[48] S.-W. Wei and Y.-X. Liu, Phys. Rev. D **105**, 104003 (2022)
[49] D. Wu, Phys. Rev. D **107**, 024024 (2023)
[50] Y.-Z. Du, H.-F. Li, Y.-B. Ma and Q. Gu, Nucl. Phys. B **1006**, 116641 (2024)